Preparation and characterisation of an aligned carbon nanotube array on the silicon (100) surface

Jingxian Yu,[a] Dusan Losic,[a] Matthew Marshall,[a] Till Böcking,[bc] John Justin Gooding[b] and Joseph George Shapter*[a]

Received 31st July 2006, Accepted 20th September 2006
First published as an Advance Article on the web 11th October 2006
DOI: 10.1039/b611016a

Arrays of aligned carbon nanotubes formed by self-assembly on a Si (100) surface are described. The surface of a Si (100) wafer has been modified by reaction of hydride-terminated Si (100) with ethyl undecylenate to give ethyl undecanoate self-assembled monolayers (SAMs) which were linked by stable silicon–carbon covalent bonds. The ester terminus of the monolayer was converted to an alcohol whereupon shortened carbon nanotubes were covalently attached using carbodiimide coupling. The formation of the SAM and its subsequent modification with nanotubes has been followed using a series of techniques including X-ray photoelectron spectroscopy (XPS), atomic force microscopy (AFM), scanning electron microscopy (SEM), IR spectroscopy and cyclic voltammetry.

Introduction

For the purpose of nanofabrication, building nanostructures and nanoelectronic devices, self-assembly (SA) is envisaged as an important avenue for fabricating and employing supramolecular nanostructures with targeting properties.[1,2] The controlled manipulation and approach of molecules to the surface is a key feature in the development of chemical-based nanotechnology. One of the interesting approaches involves the creation of densely packed highly organised monolayers on a solid substrate. Drawing inspiration from nature, building blocks may include a wide variety of molecules such as DNA, polymers, proteins, enzymes, lipids and nanoparticles.[3,4]

The most studied and the best-characterised self-assembled monolayers (SAMs) are those formed by alkanethiolates chemisorbed from solution onto gold surfaces.[5–7] They offer numerous advantages such as simple preparation, well-defined organisation, densely-packed structures and the possibility of introducing a vast number of functional groups at the monolayer surface.[8] These unique characteristics make SAMs an excellent model system for fundamental studies in surface physics, chemistry, biology and surface engineering and offer numerous applications including: optical devices, biotechnology and biosurfaces, biosensors, chemical sensors, corrosion prevention, adhesion, tribology and electrochemistry.[1,8–12]

Despite the interest in alkanethiols on gold their widespread technological application is uncertain due to issues related to long-term stability of the monolayers. Dynamic studies of alkanethiols on gold surfaces have revealed several serious disadvantages of the thiol–gold chemistry. Particularly of concern is their thermal instability,[13,14] influence of UV photooxidation,[15] evidence of the changing structures over time,[14,15] instability in solution, gold etching and adsorbate–solution interchange.[1,8,16] Critical evidence of the maturation of SAMs has shown that over a period of several months in air, there are dramatic changes in structure and integrity due to the oxidation process.[14,15]

Other more stable monolayer systems based on new substrates and non-thiol chemistry need further development. This study will explore the fabrication of monolayers based on covalent bonds as opposed to thiol chemistry based on weaker, pseudocovalent bonds which are reversible with energies of formation of 40 kcal mol^{-1}.[17] Silicon is the obvious first alternative substrate to be explored where Si–C and Si–O–C bonds are generally quite strong (80–100 kcal mol^{-1}) with surface rearrangement unlikely.[17]

In view of the importance of silicon as the primary semiconductor material in modern microelectronic devices, efforts to control its electronic properties and to tailor the chemical and physical characteristics of its surface are of major importance. One approach to this surface modification has been through the use of various siloxane-anchored self-assembled monolayers attached to the native silicon oxide by Si–O–C bonds.[1] A disadvantage of this approach is the presence of an oxidised layer and the low number of functionalised siloxanes commercially available.

To avoid these disadvantages, recently the preparation of dense alkyl monolayers covalently bonded to silicon surface has been reported.[18,19] The basic approach for monolayer formation on Si substrates is based on surface hydrogenation followed by the reaction with aliphatic alkenes. It has been shown that neat 1-alkenes react efficiently with a hydrogen-terminated silicon surface. The resulting monolayer, which is linked to the surface by very stable covalent Si–C bonds, is densely packed as evidenced from infrared spectroscopy, X-ray photoelectron spectroscopy, ellipsometry and wetting experiments.[18,20] A variety of functionalised monolayers on silicon surfaces with different lengths and functional groups on the

[a]*School of Chemistry, Physics and Earth Sciences, Flinders University, Sturt Road, Bedford Park, SA 5042, Australia*
[b]*School of Chemistry, University of New South Wales, Sydney, NSW 2052, Australia*
[c]*School of Physics, University of New South Wales, Sydney, NSW 2052, Australia*

This journal is © The Royal Society of Chemistry 2006

free end could be prepared in a simple way using this synthetic route. This provides a foundation for the assembly of nanoscale integrated systems, including the coupling of carbon nanotubes (SWCNT), enzymes and oligonucleotides,[21–23] without the stability problems of the alkanethiol system.

We are particularly interested in developing stable biomolecular interfaces where the biological molecule is efficiently connected to an electrochemical transducer. The efficient transfer of electrons between enzymes and other biomolecules to electrodes is important for developing protein-based biosensors and bioelectronic devices. For example, research into the interaction and electron exchange between redox enzymes and an electrode interface is important for two reasons: first, it is helpful to understand the intrinsic redox properties of proteins;[24,25] and second, direct electron transfer between enzymes and electrodes is the key to the development of mediatorless, also called third-generation, enzyme biosensors.

One strategy to achieve efficient electron transfer to proteins is to build up the electrode inside the protein so that it is close to the redox-active center of the protein.[26–29] To achieve this requires exceedingly small electrodes. Carbon nanotubes, which are as small as 1 nm in diameter, have the potential to be such electrodes.[29] The purpose of this paper is to demonstrate the attachment of vertically aligned cut carbon nanotubes on a stable SAM-modified silicon substrate for the first time. A schematic of the process used is presented in Fig. 1. The preparation of the silicon surface and the formation of a SAM by reaction of Si(100)–H with ethyl undecylenate is first characterised using X-ray photoelectron spectroscopy and FTIR spectroscopy whereupon the formation of nanotube arrays and their resultant electrochemistry can be followed unambiguously.

Experimental

Preparation of ethyl undecanoate terminated silicon (100) surfaces

Highly boron doped p-type silicon (100) wafers (0.5 mm thickness, 1 mΩ cm resistivity and polished on one side) were purchased from Virginia Semiconductor, Inc. USA. The surfaces (0.5 × 0.5 cm^2 size) were cleaned in acetone (99.5%, Merck), tetrahydrofuran (THF, APS Chemicals, Australia) and copious Milli Q water (18 MΩ cm), then chemically oxidised for 30 min in 100 °C 3 : 1 (v/v) H_2SO_4 (98%, APS Chemicals, Australia) : H_2O_2 (30%, AR). The hydrophilic oxidised silicon surfaces were flushed with copious Milli Q water and dried with a compressed air flow, then immersed in a previously deoxygenated and stagnant 40% NH_4F solution (Semiconductor grade, Aldrich-Sigma) for 30 min to prepare hydride-terminated surfaces.[30] During the silicon etching, high purity nitrogen was flushed above the solution to keep the environment oxygen free. HF can also be used to prepare the hydride surfaces and will yield flatter surfaces for Si (100). AFM results show that the substrates prepared using the NH_4F are flat enough for this particular application.

The resulting hydrophobic surface was washed with copious amounts of Milli Q water for several seconds and dried with high purity nitrogen flow. It was then placed quickly in a round-bottom flask and transferred into a nitrogen-filled glove-box. Two millilitres of ethyl undecylenate (97%, Aldrich stored over molecular sieve) was added into the round-bottom flask. The round-bottom flask was heated to 180 °C for 24 h using a silicone-oil bath to prepare the ethyl undecanoate monolayer modified silicon surface. The silicon surfaces were removed and rinsed repeatedly with ethanol and tetrahydrofuran to remove physisorbed materials. The hydrophobic

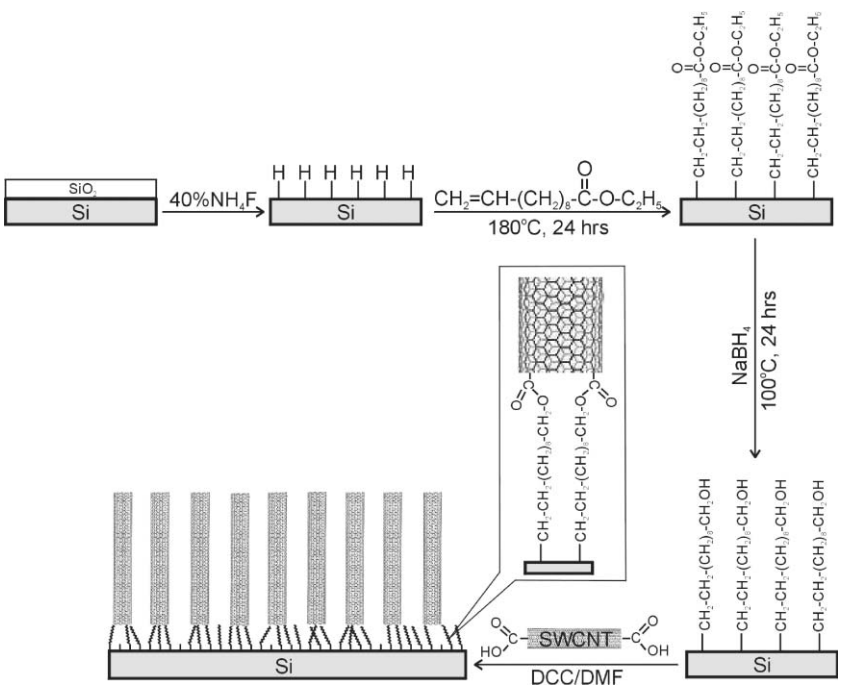

Fig. 1 Schematic representation of the process used to attach SWCNT to Si(100).

 This journal is © The Royal Society of Chemistry 2006

surfaces were then washed with copious Milli Q water and dried with a compressed air flow.

Preparation of alcohol-terminated silicon (100) surfaces

The ester modified silicon surfaces were transferred under N_2 into a round-bottom flask containing 4 ml saturated sodium borohydride 2-methoxyethyl ether solution and warmed to 100 °C for 24 h to prepare an alcohol terminated surface. Then the silicon wafers were washed with ethanol, tetrahydrofuran and copious Milli Q water and dried with high purity N_2 flow.

Preparation of an aligned carbon nanotube array on silicon (100) surfaces

The single-walled carbon nanotubes (RFP-SWCNT, Carbon Solutions, Inc. USA) were firstly shortened as described previously[26,31,32] by sonicating SWCNTs in a 3 : 1 (v/v) H_2SO_4 (98%) and HNO_3 (70%, APS Chemicals, Australia) for 8 h. To keep the temperature constant during the SWCNTs cutting, ice was added continuously. The shortened nanotubes were filtered and washed with copious amounts of Milli Q water until the pH was greater than 5. The average length of shortened SWCNTs was 360 nm determined using AFM measurements of nanotubes lying on a mica substrate.[33] One milligram of shortened SWCNT was dispersed in 5 ml dimethylformamide (DMF, 99.8%, Aldrich) with 3 mg dicyclohexyl carbodiimide (DCC, 99%, Aldrich) to convert the carboxylic groups at the ends of the shortened SWCNT into active carbodiimide esters.[26,31] The alcohol-terminated silicon was incubated in the nanotube solution for between 4 and 48 hours to give a silicon substrate modified with an array of aligned carbon nanotubes.

X-Ray photoelectron spectroscopy (XPS) measurements

X-Ray photoelectron spectra were obtained on a Leybold-Heraeus XPS spectrometer equipped with an Al K_α source (1486.6 eV). The take-off angle for detection was nominally 90° from the surface. The pressure in the main chamber was less than 5×10^{-8} torr during analysis. Spectra of the Si_{2p} (90–110 eV binding energy), C_{1s} (276–296 eV binding energy), O_{1s} (522–542 eV binding energy) regions and survey scans (0–1000 eV binding energy) were recorded. XPS peak fitting was performed using the XPSPEAK software (version 4.1).[34] In the atomic analysis, atomic sensitivity factors of 0.296, 0.711 and 0.283 were used for carbon (1s), oxygen (1s) and silicon (2p) respectively.[35]

Infrared spectroscopy

Silicon (100) plates (15 mm × 55 mm size) were placed carefully with the polished side of the wafer facing down and contacted with the flat germanium ATR crystal (50 mm × 10 mm × 3 mm size, 45° bevel angle). The analysis angle was set to 30° for the variable angle horizontal ATR accessory (Pike technologies, Inc., USA). The number of reflections in the crystal was 28. FTIR spectra were measured using a Bio-RAD FTS-40A spectrometer equipped with a MCT (mercury cadmium telluride) detector cooled with liquid nitrogen. All of the spectra were recorded by integrating 256 interferograms in the wavenumber range (1000–4000 cm^{-1}) with a resolution of 2 cm^{-1}. Reference spectra were obtained using an oxidised silicon (100) surface because the hydrogen terminated silicon surface can be contaminated easily by organic chemicals in air.[36] The Ge crystal was cleaned with neat tetrahydrofuran before every experiment, and the ATR accessory was purged with dry N_2 during data acquisition.

Electrochemical measurements

All electrochemical experiments were performed in a specially designed Teflon electrochemical cell, as described previously.[37] Hydrogen terminated silicon, ester-terminated or aligned carbon nanotube array modified silicon samples were used as working electrodes. The active area of working electrode, which is 0.075 ± 0.005 cm^2 in this work, was defined using an O-ring pressed down against the silicon samples. The electrical contact to the silicon working electrode was obtained by scratching the unpolished side of the wafer with a SiC crystal. An aluminium foil adhered well to the scratched side and maintained a stable electrical contact. A platinum mesh was used as counter electrode and a Ag/AgCl electrode was used as the reference electrode. The background electrolyte was an aqueous solution (pH = 6.8) of 0.05 mol L^{-1} KCl, 0.05 mol L^{-1} K_2HPO_4 and 0.05 mol L^{-1} KH_2PO_4. All electrochemical experiments were performed using Power Lab, model 400s (AD Instruments, Sydney, Australia) computer-controlled electrochemical system at room temperature.

Atomic force microscopy (AFM)

Atomic force microscope tapping mode images of hydrogen-terminated silicon, ester-modified silicon and aligned carbon array modified silicon were taken in air with a multi-mode head and Nanoscope IV controller (Digital Instruments, Veeco, Santa Barbara). Commercially available silicon cantilevers (FESP-ESP series, Veeco probes, Santa Barbara) with fundamental resonance frequency between 70–85 KHz were used. Topographic (height) and amplitude images were obtained simultaneously at a scan rate of 1 Hz with the parameters of set point, amplitude, scan size, and feedback control optimised for each sample. All images presented represent background subtracted data using the 'flatten' feature in the Digital Instruments software.

Scanning electron microscopy (SEM)

Prior to the SEM imaging, the sample was sputter-coated with a 2 nm thick platinum layer. Scanning electron microscope images were taken with a Philips XL30 Field Emission Scanning Electron Microscope under 10 kV accelerating voltage, at Adelaide Microscopy, University of Adelaide, South Australia. All images were scanned using the slowest scan mode for improved clarity.

Results and discussion

The steps involved in fabricating the aligned nanotube arrays on silicon surfaces are illustrated in Fig. 1. Firstly the silicon oxide layer on a silicon surface is removed *via* etching in NH_4F solution to give a hydrogen-terminated silicon surface. This

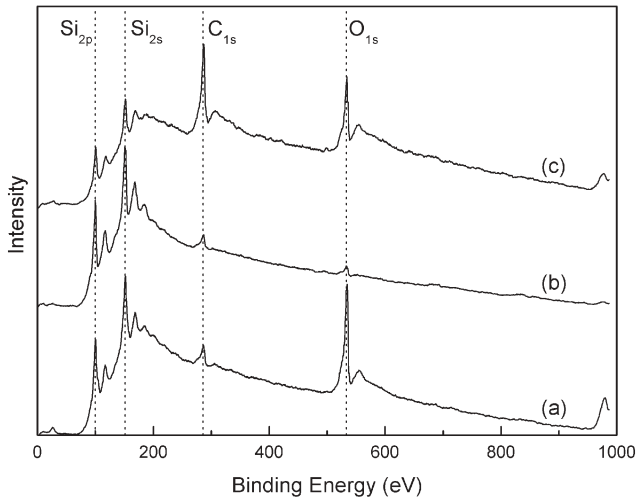

Fig. 2 X-Ray photoelectron survey spectrum at each step for the preparation of ethyl undecanoate-terminated silicon (100) surface. (a) Oxidised silicon after immersing in the piranha solution for 30 min at 100 °C. (b) Hydrogen-terminated silicon after immersing in the deoxygenated 40% NH_4F solution for 30 min at room temperature. (c) Ester-terminated silicon after immersion in the ethyl undecylenate for 24 h at 180 °C.

surface is reacted with the alkene, ethyl undecylenate to give an ethyl undecanoate self-assembled monolayer. The ester moieties at the end of the ethyl undecanoate are reduced to an alcohol using sodium borohydride. It is this surface which is coupled to the carbon nanotubes. Shortened carbon nanotubes are incubated in DCC which converts carboxylic acid moieties on the ends and defects on the walls of the SWCNTs to *O*-acylisourea intermediates. These reactive intermediates are susceptible to nucleophilic attack from the alcohol terminated SAM to give an ester bond. The end result is covalent attachment of the SWCNTs to the self-assembled monolayer modified silicon surface. In the ideal case the SWCNTs will only attach from their ends to give aligned carbon nanotube arrays.

X-Ray photoelectron spectra

Fig. 2 shows the X-ray photoelectron survey spectrum at each step for the preparation of ethyl undecanoate modified silicon (100) surface. For the oxidised silicon, a strong O_{1s} peak at binding energy 532 eV is observed in addition to Si_{2s} and Si_{2p} peaks. The high resolution spectrum for Si_{2p}, shows the peak can be deconvoluted into two peaks at binding energy 98.8 eV and 102.6 eV. The former is assigned to the single crystal silicon (100) substrate and the latter is assigned to silicon dioxide. By calculation, the atomic ratio of O : Si is 1.84 if only considering the Si_{2p} intensity at 102.6 eV, which indicates that the silicon surface was completely covered by a SiO_2 thin film as expected.

After the oxidised silicon surface was immersed in the deoxygenated 40% NH_4F solution for 30 min, the O_{1s} peak decreased significantly. Using the total Si_{2p} intensity, rather than the peak at 102.6 eV attributed to SiO_2 as above, the atomic ratio of O : Si is only 0.04 which is reduced from 0.63 in the oxidised sample indicating that the oxygen atoms on the surface were replaced mostly with hydrogen atoms. Furthermore, the high resolution Si_{2p} spectrum only reveals a single peak at binding energy 99.1 eV demonstrating the removal of the oxide and the formation of hydrogen-terminated silicon surface.

After the hydrogen terminated silicon was immersed in ethyl undecylenate at 180 °C for 24 h, the relative intensities of C_{1s} and O_{1s} peaks increased significantly compared with the Si_{2s} and Si_{2p} peaks. Fig. 3 depicts the high resolution spectra for the Si_{2p}, C_{1s} and O_{1s} regions. From the Si_{2p} spectrum (in Fig. 3(a)), we only find the peak at near 99.6 eV, which is deconvoluted into two peaks at 99.3 eV and 100 eV using the XPSPeak software. The former is assigned to the Si $2p_{\frac{3}{2}}$ component and the latter to the Si $2p_{\frac{1}{2}}$ component. The C_{1s} spectrum (in Fig. 3(b)) is deconvoluted into 3 peaks at binding energy 284.5 eV, 287.1 eV and 288.9 eV. The former peak can be assigned to the carbons of the alkyl chain and the methyl group and latter to the C–O and C=O carbons of the ester group, respectively. The area ratio of the peaks is 11 : 1 : 1 for C–C : C–O : C=O, which is the expected atomic ratio of carbon atoms in the alkyl chain and ester group of the ethyl undecanoate molecule. Furthermore, the atomic ratio of C : O is approximately 13 : 2.9, which is slightly smaller than the ratio of 13 : 2 expected for the ester terminated monolayer. The larger than expected oxygen content may be due to the presence of low levels of silicon dioxide (which are not detectable in the Si_{2p} narrow scan). This result provides evidence that the changes in X-ray photoelectron spectra from curve b to curve c in Fig. 2 come from the formation of an ethyl undecanoate monolayer on the silicon surface.

Fig. 4 shows X-ray photoelectron survey spectra for the aligned carbon nanotube array on silicon surfaces for different

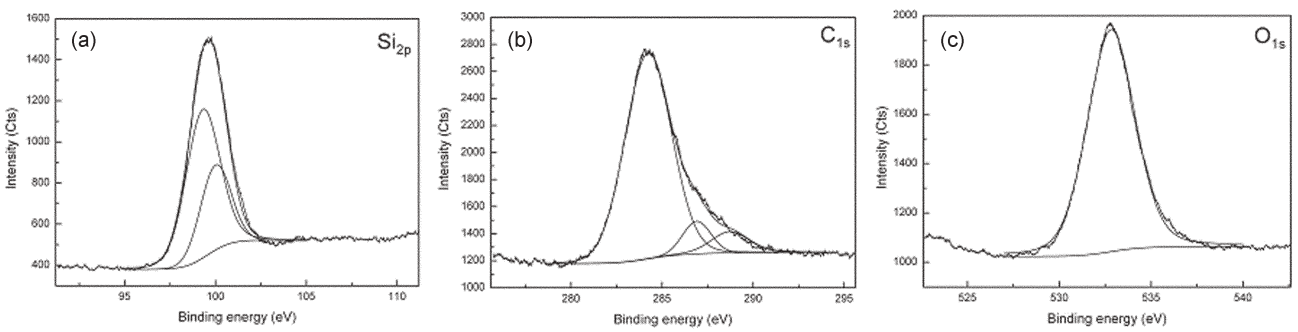

Fig. 3 High resolution X-ray photoelectron spectra of the (a) Si_{2p}, (b) C_{1s} and (c) O_{1s} regions for ethyl undecanoate-terminated silicon surface.

 This journal is © The Royal Society of Chemistry 2006

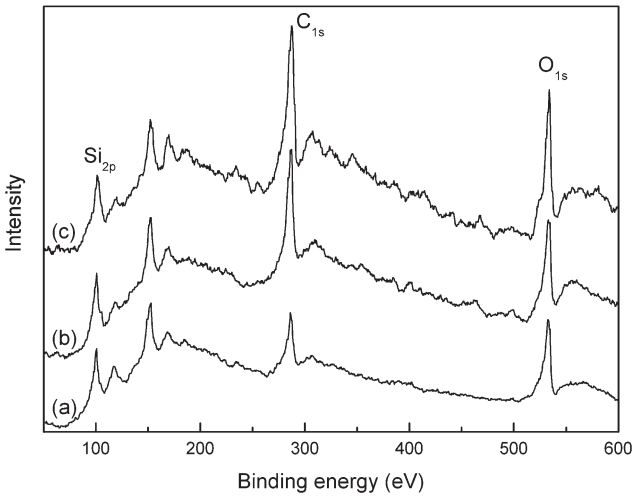

Fig. 4 X-Ray photoelectron survey spectra for the aligned carbon nanotube array on silicon (100) surfaces after immersing in the SWCNT–DMF solution for different times and at different temperatures, where all spectra were normalised relative to the intensity of the Si_{2p} peak. (a) 24 h, room temperature (b) 48 h, room temperature (c) 7 h, 100 °C.

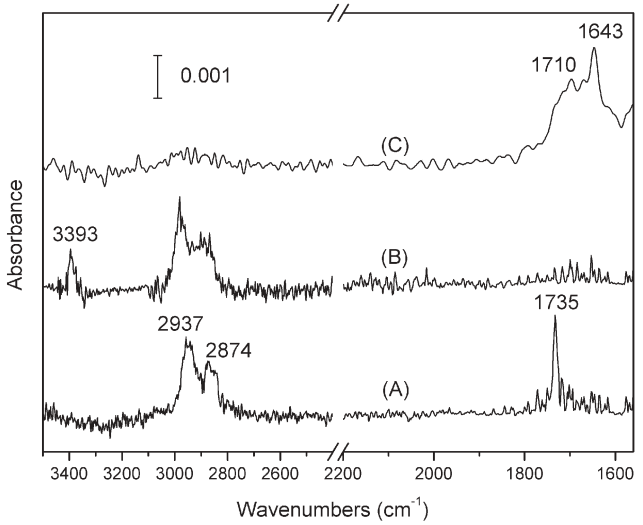

Fig. 5 ATR IR spectra at various stages of substrate production. (a) Ethyl undecanoate surface, (b) alcohol terminated surface and (c) aligned SWCNT array.

reaction times and temperatures. As reaction time and temperature increase, the intensity of C_{1s} and O_{1s} peaks increases and simultaneously the intensity of Si_{2s} and Si_{2p} decreases. By calculation, the atomic ratio of C : Si for Curve a, b and c in Fig. 4 are 1.2, 2.9 and 3.2 respectively. This indicates that more tubes are attached to the silicon surface with increasing reaction time and temperature.

The relative carbon to silicon intensity in Fig. 4(a)) is lower than in Fig. 2(c)). This might not be expected as the spectrum in Fig. 4(a)) is the same surface as in Fig. 2(c)) except with some carbon nanotubes adsorbed on the top. It is hypothesised that this change in intensity is due to the fact that the SAM has been disrupted during the attachment chemistry. The main effect of this is to create some bare Si not present when only the SAM layer was adsorbed. This increases the Si signal hence lowering the C : Si ratio. This interpretation is supported by the electrochemistry results later in this section.

Infrared spectroscopy of the shortened SWCNT array on silicon surface

The FTIR spectrum of the Si substrate is shown for each stage of the process in Fig. 5. The peaks in both the ethyl undecanoate (Fig. 5(a)) and alcohol terminated surface (Fig. 5(b)) are the expected peaks for those molecules. The IR spectrum of the surface after formation of the ethyl undecanoate monolayer shows the asymmetric and symmetric methylene stretching vibrations at 2937 and 2874 cm^{-1} respectively and the carbonyl stretching vibration at 1735 cm^{-1}. Reduction of the terminal ester groups of the monolayer to an alcohol result in the disappearance of the carbonyl stretch while the methylene stretching vibrations are still detectable. The presence of carboxylic acid groups for the covalent coupling of the nanotubes to the monolayer was confirmed by FTIR spectroscopy of SWCNTs shortened in a mixture of sulfuric and nitric acid for 8 hours. The spectrum for the shortened SWCNT array modified silicon surface is shown in Fig. 5(c). The peak at 1710 cm^{-1} is attributed to ν(C=O) in the functionalised nanotubes while that at 1643 cm^{-1} is due to quinone type units along the side walls of the nanotubes.[38,39] These assignments are supported both by the IR spectrum of unattached nanotubes[40] and the fact that they are not present until the nanotubes are added. Upon adsorption onto the surface the ν(C=O) peak shifts to slightly lower wavenumbers (1720 cm^{-1} versus 1710 cm^{-1} in the adsorbed state). This has been observed previously and is attributed to increased hydrogen bonding.[38,41] Given the condensation of the nanotubes into a densely packed self assembled layer, it is not surprising to see an increase in intermolecular interactions.

Atomic force microscopy and scanning electron microscopy

Fig. 6 and 7 show AFM and SEM images respectively of the aligned carbon nanotube array on the silicon surface after the alcohol-terminated silicon was immersed in the SWCNT–DMF solution for varying periods of time. Before adsorption of shortened SWCNTs, both the hydrogen-terminated and ethyl undecanoate modified silicon pieces show flat surfaces. After absorption, round protrusions are clearly observed on the silicon surface. The characteristics of the observed nanotubes are summarised in Table 1. As expected, the surface coverage increases with time and the values determined by AFM and SEM are in very good agreement with each other. In addition, the average length and size of the observed nanotube bundles also increase with time. The increase in feature length and thickness is attributed to the initially attached nanotubes acting as sites for subsequent tubes to adsorb to the surface. That is, once a nanotube is coupled to the surface, subsequent nanotubes can adhere to the sides of the attached nanotube. The consequence will be not only an increasing diameter but also increased length of features due to the distribution of nanotube lengths and the new tubes being able to adsorb at any point along the length of the coupled nanotubes.

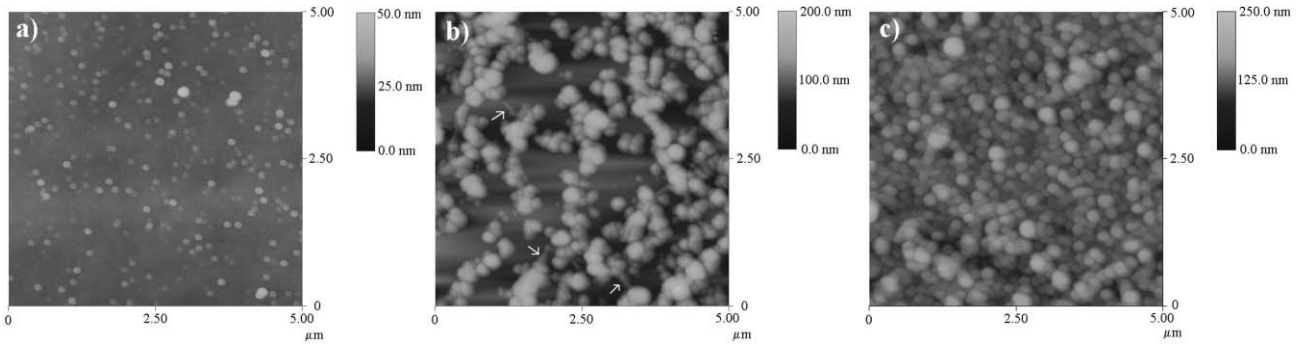

Fig. 6 AFM images of aligned carbon array on silicon surfaces after the alcohol-terminated silicon was immersed in the SWCNT–DMF solution for different times at room temperature. (a) 4 h (b) 24 h (c) 48 h. Arrows indicate nanotubes lying horizontally on the substrate.

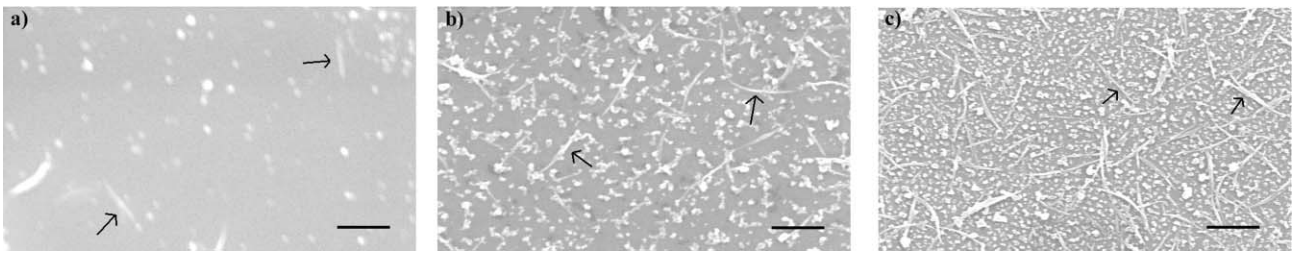

Fig. 7 SEM images of aligned carbon array on silicon surfaces after the alcohol-terminated silicon was immersed in the SWCNT–DMF solution for different times at room temperature. The scale bar is 1 μm. (a) 4 h (b) 24 h (c) 48 h. Arrows indicate nanotubes lying horizontally on the substrate.

Table 1 Characteristics of features observed after attachment of carbon nanotubes

	Fraction of surface covered		Characteristics of nanotube bundles			
Reaction time/h	AFM	SEM	Average diameter from AFM/nm	Average diameter from SEM/nm	Average height/nm	Maximum height/nm
4	0.11	0.099	111	91	3.0	28
24	0.42	0.41	250	115	49	175
48	0.87	0.70	292	123	65	204

The diameter of nanotube bundles measured by AFM is larger than that measured by SEM. This is not unexpected and is due mostly to the convolution of the tip diameter with the features being observed. In addition, at higher coverages it is difficult for the tip to fully resolve bundles in close proximity and hence some bundles are not separated in the images leading to larger average sizes.

The heights observed for the protruding nanotubes are considerably shorter than the known distribution of lengths of the cut nanotubes which for 8 hours cutting have an average nanotube length of 380 nm and a maximum observed length of about 850 nm. This has been observed previously by various workers.[26,31,42] All the SEM images and the 24 hour AFM images show features which are ascribed to nanotubes lying down (as indicated by arrows in Fig. 6 and 7). There are several possible explanations for this observation but the most likely is that the nanotubes have not only end functionalisation but side wall functionalisation as well. The cutting procedure used in these experiments is quite a strong oxidising environment known to create side wall defects.[38] The observation of a strong quinone peak in the IR spectrum of the cut nanotubes indicates that sidewall functionalities exist. The outcome of all these factors is that many of the nanotubes will be lying down on the substrate.

It is perhaps surprising that the nanotubes lying down are not observed in the AFM images at the highest coverage even though the SEM images clearly show their presence. The horizontal tubes are obvious in both AFM and SEM for the 24 hour reaction. The lack of an observation in the 48 hour AFM image is due to both the increased coverage and height of the features. Both these factors mean it is more difficult for the tip to reach the substrate between features and resolve any nanotubes lying on the substrate. As seen in the SEM image, it is possible that nanotubes could be lying across the top of previously deposited vertical bundles. The roughness of the surface caused by bundles of various lengths makes it very difficult to observe these nanotubes using AFM.

Cyclic voltammograms

To further understand the electrochemical reactivity of different silicon surfaces, we investigated their cyclic voltammetric behaviour in phosphate buffer solution. Fig. 8 shows three successive cyclic voltammograms of the

 This journal is © The Royal Society of Chemistry 2006

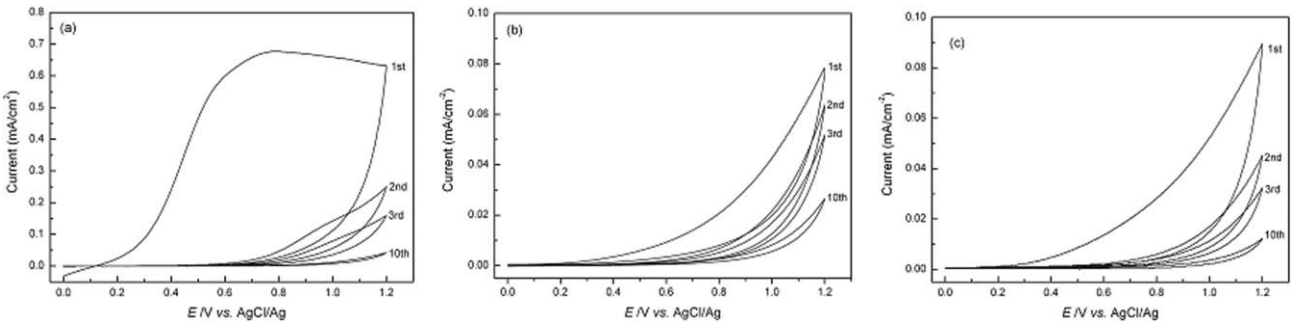

Fig. 8 Successive cyclic voltammograms of different silicon surfaces in phosphate buffer solution (scan rate 100 mV s^{-1}); (a) hydrogen-terminated silicon, (b) ethyl undecanoate-terminated silicon and (c) the aligned carbon nanotube array terminated silicon after immersing in the SWCNT–DMF solution for 24 hours at room temperature.

hydrogen-terminated silicon, ethyl undecanoate modified silicon and aligned carbon nanotube array modified silicon surfaces. It can be seen that the hydrogen terminated silicon has the highest peak current density at the first cycle, which is 0.7 mA cm^{-2} appearing at 0.7 V. The oxidation current is assigned to the formation of SiO_2 film on the surface. With increasing time, the SiO_2 film thickens. Because the SiO_2 is insulating, the oxidation current decreases with cycle number.

The cyclic voltammograms for the ethyl undecanoate modified and aligned carbon nanotube array modified silicon surfaces show significant blocking of the oxidation current. The currents for both are one order magnitude less at the first cycle than that of the hydrogen terminated surface. The aligned carbon nanotube array modified silicon exhibits slightly larger charge density in the anodic direction of the first cycle relative to the ethyl undecanoate modified surface (0.279 mC cm^{-2} integrated current for the nanotube surface *versus* 0.223 mC cm^{-2} for the ethyl undecanoate modified surface). However, the aligned nanotube array exhibited a faster decrease in current density with increasing cycle number. For example, the integrated current for the second cycle was 0.0917 mC cm^{-2} for the nanotube modified surface whilst it was 0.115 mC cm^{-2} for the ester surface. For the ester modified silicon, because the monolayer is orderly and regular, the dissolved oxygen can only reach the silicon substrate with some difficultly to oxidise the hydrogen atoms. After the adsorption of shortened SWCNTs, the SAM layer appears to be disrupted as evidenced both by the higher initial current and its more rapid decay. This is certainly partially because the carboxylic groups at one end of the shortened SWCNT (1.4 nm in diameter) can react with more than 8 alcohol molecules and hence the SAM may become more disordered.

Additionally, some nanotubes could simply penetrate the SAM to maximise van der Waals forces between the hydrophobic walls of the nanotubes and the non-polar alkyl chains of the SAM. In this way, the nanotubes would form conducting channels through the SAM and cause more rapid oxidation of the underlying silicon compared with the SAM alone as observed. Some evidence for carbon nanotubes disrupting and penetrating a long chain alkanethiol SAM comes from an electrochemical study of aligned carbon nanotubes assembled onto a gold electrode modified with an 11-amino-*n*-undecylmercaptan SAM.[43] A SAM of this length would normally be expected to passivate the electrode significantly but after assembly of the nanotube array the electrochemistry is reminiscent of an electrode where the SAM is absent. If the integrity of the SAM was maintained its passivating ability would still be evident.

Conclusion

Carbon nanotubes have been successfully attached to a silicon substrate *via* the covalent attachment of a self-assembled monolayer. The amount of nanotubes observed increases with reaction time as expected and the nanotubes appear to form bundles consistent with other observations. Electrochemistry has been used to determine the passivation of the electrode both before and after the addition of nanotubes. This passivation means that the approach of attaching nanotubes to Si using long-chain SAMs will not be appropriate as a means of transferring electrons from a reaction site, such as in a redox protein, to the substrate *via* vertically-aligned nanotubes.

References

1 J. L. Wilbur and G. M. Whitesides, in *Self-assembly and self-assembled monolayers in micro and nanofabrication, nanotechnology*, ed. G. Timp, Springer-Verlag, New York, 1999, ch. 8.
2 J. A. Rogers, R. J. Jackman and G. M. Whitesides, *J. Microelectromech. Syst.*, 1997, **6**, 184–192.
3 M. Mrksich and G. M. Whitesides, *Trends Biotechnol.*, 1995, **13**, 228–235.
4 M. Mrksich and G. M. Whitesides, *Annu. Rev. Biophys. Biomol. Struct.*, 1996, **25**, 55–78.
5 R. G. Nuzzo and D. L. J. Allara, *J. Am. Chem. Soc.*, 1983, **105**, 4481–4483.
6 A. Ulman, *Chem. Rev.*, 1996, **96**, 1533–1554.
7 L. H. Dubois and R. G. Nuzzo, *Annu. Rev. Phys. Chem.*, 1992, **60**, 437–463.
8 H. O. Finklea, *Electroanal. Chem.*, 1996, **19**, 109–335.
9 A. Ulman, *An Introduction to Ultrathin Organic Films From Langmuir–Blodgett to Self-Assembly*, Academic Press, Inc., London, 1991.
10 J. Ricket, T. Weiss and W. Gopel, *Sens. Actuators, B*, 1996, **31**, 45–50.
11 J. J. Gooding and D. B. Hibbert, *TrAC, Trends Anal. Chem.*, 1999, **18**, 525–533.
12 J. J. Gooding, W. R. Yang, F. J. Mearns and J. Q. Liu, *Electroanalysis*, 2003, **15**, 81–96.
13 E. Delamarche, B. Michel, H. Kang and C. Gerber, *Langmuir*, 1994, **10**, 4103–4108.
14 A. B. Horn, D. A. Russell, L. J. Shorthouse and T. R. E. Simpson, *J. Chem. Soc., Faraday Trans.*, 1996, **92**, 4759–4762.

15 M. H. Schoenfisch and J. E. Pemberton, *J. Am. Chem. Soc.*, 1998, **120**, 4502–4513.
16 F. P. Zamborini and R. M. Crooks, *Langmuir*, 1998, **14**, 3279–3286.
17 R. L. McCreery, *Chem. Mater.*, 2004, **16**, 4477–4496.
18 M. R. Linford, P. Fenter, P. M. Eisenberger and C. E. D. Chidsey, *J. Am. Chem. Soc.*, 1995, **117**, 3145–3155.
19 A. B. Sieval, A. L. Demirel, J. W. M. Nissink, M. R. Linford, J. H. van der Maas, W. H. de Jeu, H. Zuilhof and E. J. R. Sudholter, *Langmuir*, 1998, **14**, 1759–1768.
20 A. B. Sieval, R. Linke, H. Zuilhof and E. J. R. Sudholter, *Adv. Mater.*, 2000, **12**, 1457–1460.
21 T. Böcking, M. Gal, K. Gaus and J. J. Gooding, *Aust. J. Chem.*, 2005, **58**, 660–663.
22 T. Böcking, K. A. Kilian, T. Hanley, S. Ilyas, K. Gaus, M. Gal and J. J. Gooding, *Langmuir*, 2005, **21**, 10522–10529.
23 T. Böcking, K. A. Kilian, K. Gaus and J. J. Gooding, *Langmuir*, 2006, **22**, 3494–3496.
24 A. Heller, *Acc. Chem. Res.*, 1990, **23**, 128–134.
25 E. Katz and I. Willner, *ChemPhysChem*, 2004, **5**, 1084–1104.
26 J. J. Gooding, R. Wibowo, J. Liu, W. Yang, D. Losic, S. Orbons, F. J. Mearns, J. G. Shapter and D. B. Hibbert, *J. Am. Chem. Soc.*, 2003, **125**, 9006–9007.
27 J. Liu, A. Chou, W. Rahmat, M. N. Paddon-Row and J. J. Gooding, *Electroanalysis*, 2005, **17**, 38–46.
28 X. Yu, D. Chattopadhyay, I. Galeska, F. Papadimitrakopoulos and J. F. Rusling, *Electrochem. Commun.*, 2003, **5**, 408–411.
29 J. J. Gooding, *Electrochim. Acta*, 2005, **50**, 3049–3060.
30 P. Allongue, C. H. de Villeneuve, S. Morin, R. Boukherroub and D. D. M. Wayner, *Electrochim. Acta*, 2000, **45**, 4591–4598.
31 Z. Liu, Z. Shen, T. Zhu, S. Hou, L. Ying, Z. Shi and Z. Gu, *Langmuir*, 2000, **16**, 3569–3573.
32 J. Liu, A. G. Rinzler, H. J. Dai, J. H. Hafner, R. K. Bradley, P. J. Boul, A. Lu, T. Iverson, K. Shelimov, C. B. Huffman, F. Rodriguez-Macias, Y. S. Shon, T. R. Lee, D. T. Colbert and R. E. Smalley, *Science*, 1998, **280**, 1253–1256.
33 M. W. Marshall, S. Popa-Nita and J. G. Shapter, *Carbon*, 2006, **44**, 1137–1141.
34 R. Kwok, *XPSPEAK 4.1 Users Guide*, 2000, download from http://www.phy.cuhk.edu.hk/~surface/XPSPEAK/.
35 J. F. Moulder, W. F. Stickle, P. E. Sobol, K. D. Bomben and J. Chastain, *Handbook of X-ray Photoelectron Spectroscopy*, Perkin-Elmer Corporation, Eden Prairie, MN, 1992, p. 252.
36 S. Ye, T. Ichihara and K. Uosaki, *Appl. Phys. Lett.*, 1999, **75**, 1562–1564.
37 D. Losic, J. J. Gooding, J. G. Shapter, D. B. Hibbert and K. Short, *Electroanalysis*, 2001, **13**, 1385–1393.
38 J. Zhang, H. Zou, Q. Qing, Y. Yang, Q. Li, Z. Liu, X. Guo and Z. Du, *J. Phys. Chem. B*, 2003, **107**, 3712–3718.
39 D. B. Mawhinney, V. Naumenko, A. Kuznetsova, J. T. Yates, Jr., J. Liu and R. E. Smalley, *J. Am. Chem. Soc.*, 2000, **122**, 2383–2384.
40 A. Chou, T. Böcking, N. K. Singh and J. J. Gooding, *Chem. Commun.*, 2005, 842–844.
41 T. Hemraj-Benny, S. Banerjee and S. S. Wong, *Chem. Mater.*, 2004, **16**, 1855–1863.
42 B. Wu, J. Zhang, Z. Wei, S. Cai and Z. Liu, *J. Phys. Chem. B*, 2001, **105**, 5075–5078.
43 P. Diao, Z. F. Liu, B. Wu, X. L. Nan, J. Zhang and Z. Wei, *ChemPhysChem*, 2002, **3**, 898–901.

 This journal is © The Royal Society of Chemistry 2006